A novel insect-inspired optical compass sensor for a hexapod walking robot

Julien Dupeyroux, Julien Diperi, Marc Boyron, Stéphane Viollet, Julien Serres

A novel insect-inspired optical compass sensor for a hexapod walking robot*

Julien Dupeyroux[1], Julien Diperi[1], Marc Boyron[1], Stéphane Viollet[1] and Julien Serres[1]

Abstract—In an outdoor autonomous navigational context, classic compass sensors such as magnetometers have to deal with unpredictable magnetic disturbances. In this paper, we propose to get inspiration from the insect navigational abilities to design a celestial compass based on linear polarization of ultraviolet (UV) skylight. To compute the solar meridian relative orientation, our 3D-printed celestial compass uses only two pixels created by two UV-light photo-sensors topped with linear polarizers arranged orthogonally to each other, in the same manner that was observed in insects' Dorsal Rim Area ommatidia. The compass was then embedded on our hexapod walking robot called Hexabot. We first tested the UV-polarized light compass to compensate for yaw random disturbances. We then used the compass to maintain Hexabot's heading direction constant in a straight-forward task, knowing the robot has important yaw drifts. Experiments under various meteorological conditions provided steady state heading direction errors from $0.3°$ under clear sky conditions to $1.9°$ under overcast sky, which suggests interesting precision and reliability to make this optical compass suitable for robotics.

I. INTRODUCTION

Navigation systems such as Inertial Measurement Units (IMUs) embedded on robots, smart-phones and so on, generally include magnetometers providing an absolute heading direction relative to the Earth's magnetic field. However local magnetic fields produced by ferrous materials can cause incorrect magnetometer measurements. The classical approaches to magnetic disturbances compensation rely on Kalman filtering and require sensor fusion from gyroscopes and accelerometers [1]. It is well known that gyroscopes and accelerometers are also prone to drifts. Therefore, the solutions currently proposed remain sensitive to multiple sources of disturbances. In complex outdoor environments where magnetic interferences are increasingly present and often unpredictable, it would be interesting to benefit from a new way to get a reliable measurement of heading direction.

Biomimetic approach has led to interesting models for optimization, control and automation in robotics. We propose here to get inspiration from the insects' skylight polarization compass [2] to provide a reliable measurement of the heading direction.

The polarization pattern of skylight is caused by the scattering phenomenon within the Earth's atmosphere. Indeed, solar radiations remain unpolarized until their entry into the atmosphere. Scattering interactions with atmospheric constituents induce the partially linear polarization of the skylight [3]. As shown in figure 1, the direction of the linear polarization of skylight at the zenith point is always perpendicular to the solar meridian. During daytime, the sun path makes the polarization pattern rotate around the zenith at an average speed of $15°$ per hour. The sun path is not constant and depends not only on the position of the Earth about the sun, but also on the location of the observer.
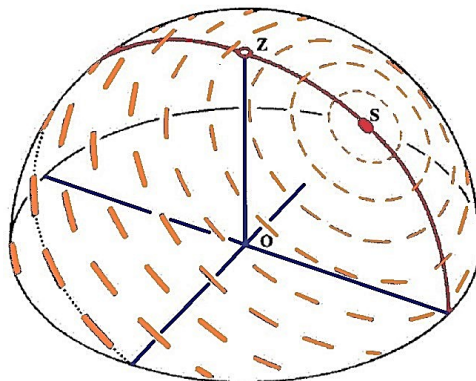

Fig. 1. Three dimensional representation of the polarization of skylight seen from an observer (O). The red curve crosses zenith point (Z) relative to observer, and sun point (S). The solar meridian is the part of red curve that starts from the zenith and crosses the sun. The anti-solar meridian is the symmetric part of the curve. Orange lines' orientation and thickness show the direction and the degree of polarization respectively. Adapted from [4].

Studies showed the existence of ommatidia sensitive to the polarization of skylight in the insect's compound eye [5]. Electro-physiological recordings from the cricket showed that these particular ommatidia are restricted to the upper side of the compound eye : the Dorsal Rim Area (DRA) [6]. Many other insects exhibit the same polarization sensitivity, such as the desert locust, the monarch butterfly, the fruit fly [7], and honeybees [8]. For all species whose DRA was identified, each ommatidium is sensitive to a unique direction of polarization and its orthogonal direction, though the exact anatomical structure differs between species. The spectral sensitivity of the DRA is generally in the UV light, except for a few species whose maximal sensitivity is in the blue range or in the green range. Many hypotheses have been proposed to explain why ommatidia are sensitive to UV light instead of other spectral ranges. The most reasonable assumption is that the skylight polarization remains strong in the UV under canopies and clouds [9], [10].

From a neural standpoint, for instance in the locust brain, the information perceived through the DRA is first integrated

by polarization neurons, called POL-neurons, in the optic lobe, which show a high synaptic activity for three distinct angles ($10°$, $60°$ and $130°$). In the central complex, POL-neurons show a rather uniform synaptic activity for all polarization directions from $0°$ to $360°$ [11], [12]. A *winner takes all* mechanism can be used to understand how the heading direction is retrieved in the central complex of an insect [8], [13]. DRA-based neural models mostly provide an estimated heading direction by computing the logarithmic difference between response of the ommatidium to a single polarization orientation, and the response of the same ommatidium to the corresponding orthogonal polarization orientation [6].

End-use analyses of the celestial compass found in desert ants or in honeybees show that insects tend to refer to a unique, global polarization direction angle [14] in order to get their bearings. For instance, during a foraging trip in an unknown place, desert ants Cataglyphis integrate their heading direction through their celestial compass. Although their foraging trip consists of a slightly random exploration trajectory, their homing trajectory tends to be direct and straight to the nest [14].

In the late 1990s, Lambrinos et al. created the first wheeled robot, named Sahabot 1, integrating a celestial compass [15] which spectral sensitivity ranges from $400nm$ to $520nm$ (like in the DRA of the cricket). The project sought to test three different models to get the heading direction: (i) the scanning model uses only one polarization sensor and makes the robot rotate to find the highest sensor response and thus get the heading direction. However, the rotating phase can induce 2D displacements and therefore increase the final position error in a navigational context, (ii) the extended scanning model uses the same procedure as the scanning model but with three polarization sensors set at different orientations ($0°$, $60°$ and $120°$). The heading direction is then computed simply by subtracting the sensor signals. This method provides more reliable results since peaks detected at the corresponding linear polarization angle are sharper than in the scanning model, (iii) the simultaneous model, uses three polarization sensors without rotating the robot. Logarithmic differences are computed between each sensor so that the heading direction can be correctly estimated. Tests were performed in the early morning and the average angular error was of $0.66°$ using the simultaneous model, and $1.73°$ using the simple scanning model. The simultaneous model was then applied to Sahabot 2 in order to implement ant inspired path integration models [16].

Chu et al. developed a celestial compass based on the one integrated in the Sahabot projects, using the simultaneous model [17], [18]. The compass was embedded onto a wheeled robot using a fuzzy logic controller to follow a preprogrammed trajectory. Tests were performed at the end of the day to prevent any photo-sensors saturation. A miniaturized version of the celestial compass has also been proposed [19] but no implementation onto a mobile robot has been recorded.

Another implementation of the celestial compass has been embedded on a small Unmanned Aerial Vehicle (UAV) [20].

Three polarization sensors, including effective directions and their corresponding orthogonal, were integrated in an ocelli based autopilot designed to control the UAV roll and pitch over ten seconds of flight.

It is still unclear how insects distinguish solar and anti-solar angles. Sahabot simply integrated the position of the sun to avoid any ambiguity [15], [16], but some suggest that insects use a circadian clock to both dispel the heading direction ambiguity and compensate the sun path [21].

In this study, we propose to merge both scanning and simultaneous models proposed by Lambrinos et al. [15] into a UV-polarized light scanning model providing highly accurate measurement of the heading direction of our walking robot under various meteorological conditions and a low UV-index[1]. Section II presents the UV-polarized light compass. Section III describes the hexapod walking robot. Section IV examines two practical experiments of heading direction recovery using our celestial compass in real outdoor conditions and under various weather conditions.

II. THE UV-POLARIZED LIGHT COMPASS

A. The 3D-printed UV-polarized light sensor

The celestial compass uses two UV-light sensors (SG01D-18, SgLux) mounted below rotating UV linear sheet polarizers (HNP'B replacement) held by 70-teeth gears (fig. 2.b). Both gears are driven by a third one composed of 10 teeth and actuated by a stepper motor (AM0820-A-0,225-7, Faulhaber). Due to its symmetric properties, the two UV sheet polarizers holder gears turn in the same direction. The entire prototype was printed using PLA filament (polyactic acid). The angular resolution of the compass can be modified by changing the micro-step settings of the stepper motor. The angular resolution was arbitrarily set to $1.29°$ for all the experiments introduced in this paper.

We call POL-sensor any polarization sensor system composed of a UV sheet polarizer and a UV-light photo-receptor. The left POL-sensor is called UV_0 and the right one is called UV_1. Let x be the rotation angle of the UV sheet polarizer holder gears, and ψ the solar meridian direction angle. According to the polarization pattern in the skydome, UV_0 and UV_1 are π-periodic sinusoidal functions of x, as decribed below:

$$\begin{cases} UV_0(x) = A_0 + B_0 \cdot cos(2(x+\psi)) \\ UV_1(x) = A_1 + B_1 \cdot cos(2(x+\psi+\frac{\pi}{2})) \end{cases} \quad (1)$$

where $x \in [0; 2\pi]$ and $\psi \in [0; \pi]$, A_0 and A_1 are offsets determined by the average UV-light radiance and inner bias of each photo-sensor, B_0 and B_1 are constants determined by the degree of polarization and inner gain of each photo-sensor. In case of bad weather conditions, B_0 and B_1 values are significantly reduced due to the weakening of the degree of polarization, implying heavy noise disturbances in POL-sensors measurements (see fig. 3).

---

[1]Experiments conducted with Sahabot were done in desert conditions whith high UV range (UV-index of 11 in Maharès, Tunisia, in August 1996). Source: http://www.temis.nl/uvradiation/UVindex.html
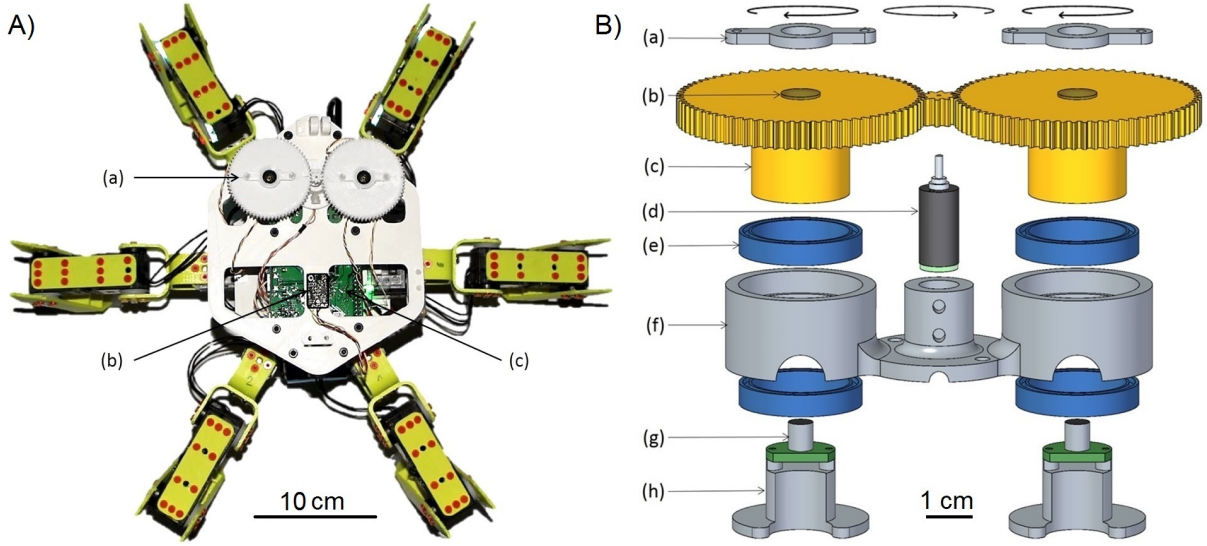
Fig. 2. **A**. Top view of the Hexabot robot equipped with the UV-polarized light compass. (a) UV-polarized light compass; (b) MinImu-9 v.3 gyro, accelerometer & compass (Pololu) used for ground truth measurement of absolute heading direction; (c) Raspberry Pi 2B board. **B**. An exploded view of the UV-polarized light compass. (a) 3D-printed fixation (PLA, polyactic acid) for the UV sheet polarizer; (b) UV linear sheet polarizer (HNP'B replacement, UV grade $275-750nm$); (c) 3D-printed gears (PLA); (d) stepper motor AM0820-A-0,225-7 (Faulhaber); (e) ball bearing; (f) 3D-printed support (PLA) for gears, ball bearings and stepper motor; (g) UV-light sensor SG01D-18 (SgLux); (h) 3D-printed support (PLA) for UV-light sensor.

A low-pass filter is then applied to the signals which only the first harmonic is kept. According to equation (1), the expected signal $UV(x)$ must be an offset, amplified sinuoidal function. Therefore, the first harmonic of its spectrum, which holds the maximum of energy, must be the best representative signal without noise. Let UV_0^{nc} and UV_1^{nc} be the normalized and corrected of the UV_0 and UV_1 POL-sensor raw signals, computed following the algorithm below:

Algorithm 1 Correction and normalization of the raw signals

1: **for** $\texttt{i} \in [0:1]$ **do**
2: $\quad \widehat{UV_i} = \boldsymbol{DFT}(UV_i)$
3: $\quad \widehat{UV_i}[2:length(\widehat{UV_i})/2] = 0$
4: $\quad UV_i^n = \boldsymbol{abs}(\boldsymbol{rDFT}(\widehat{UV_i}))$
5: $\quad UV_i^{nc} = UV_i^n - \boldsymbol{min}(UV_i^n) + \varepsilon$
6: $\quad UV_i^{nc} = UV_i^{nc}/\boldsymbol{max}(UV_i^{nc})$

---

where $\boldsymbol{DFT}$ and $\boldsymbol{rDFT}$ are respectively the direct and reverse Discrete Fourier Transform functions, and $\varepsilon = 0.0001$ is arbitrarily set to prevent from logarithm calculation failure.

The POL-unit response $p(x)$ is defined as

$$p(x) = log_{10}\left(\frac{UV_1^{nc}(x)}{UV_0^{nc}(x)}\right) \qquad (2)$$

The solar meridian direction ψ is then calculated by locating the two local minimum values of the p function, the first one being in $[0;\pi]$ and the second one in $[\pi;2\pi]$:

$$\psi = \frac{1}{2}\left[\underset{x\in[0;\pi]}{\arg\min} p(x) + \left(\underset{x\in[\pi;2\pi]}{\arg\min} p(x) - \pi\right)\right] \qquad (3)$$

The knowledge of ψ is restricted to $[0;\pi]$ due to the symmetry of the polarization pattern around the zenith point.

Classical methods to eliminate the ambiguity between ψ_{Solar} and $\psi_{Anti-Solar}$ use the ambient radiance distribution [15], [16]. As none of the tasks asked from the robot imply a turn back movement, there were no reason for ψ to change for $\psi + \pi$. Therefore, we always assumed that $\psi \in [0;\pi]$. Using the average value of the two minima of function p provides more accuracy in determining the solar meridian direction angle.

B. Sensor characteristics

The UV-light sensor is SG01D-18 (SgLux). Its active area is equal to $0.5mm^2$ and its spectral sensitivity is between $200nm$ and $375nm$ with a maximum spectral response at $280nm$. Due to the positioning of each component of the UV-polarized light compass, the full angular field of view of a POL-sensor is equal to $100°$. The refresh rate of each POL-sensor is $33.3Hz$.

The UV linear sheet polarizer has a local maximum single (respectively parallel) UV-light transmission of 52% (respectively 27%) for wavelengths from $270nm$ to $400nm$, with a peak transmission located at $\lambda \approx 330nm$.

C. POL-unit signal processing

Typical signals acquired with our celestial compass are shown in figure 3. These results were obtained on Feb. 9, 2017 at 11:36 am. The UV-index was equal to 1 according to the French meteorological services and the whole sky was covered with clouds hiding the sun. Through a 42-second acquisition time, the signal magnitude does not remain constant as a result of little changes in weather. The degree of polarization varies in function of the height of clouds crossed by the light, or partial clearing of the sky. Under clear sky conditions, the peak-to-peak magnitude of the UV signals
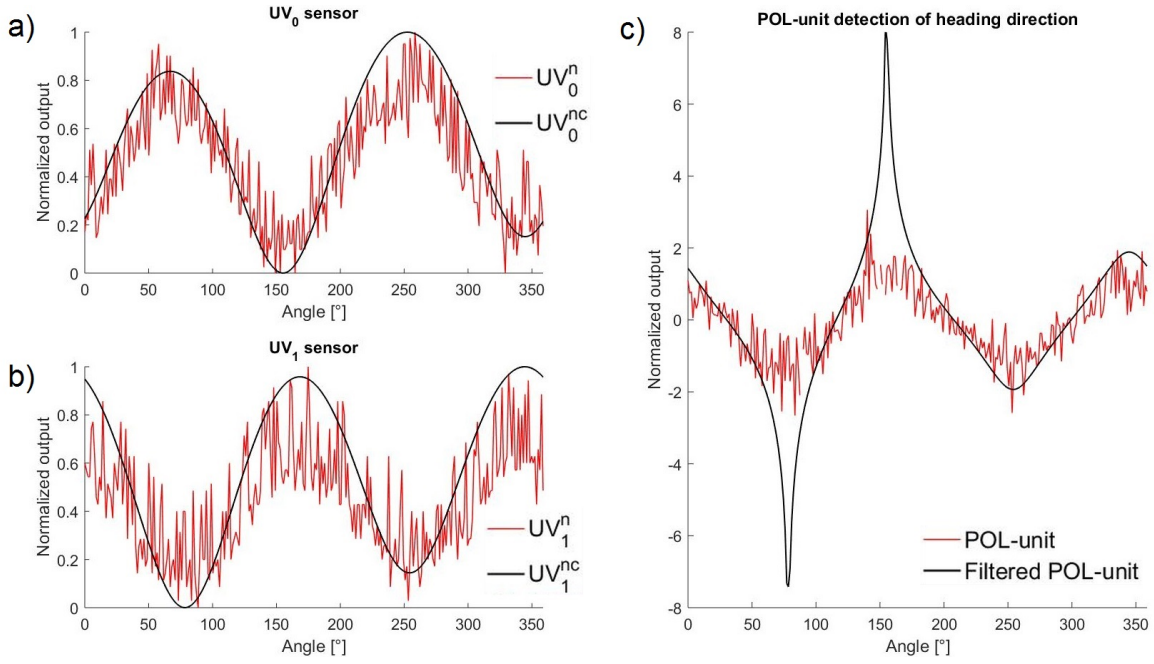
Fig. 3.   Example of signals obtained during one acquisition from the UV-polarized light compass. (a) and (b) show normalized raw (UV_0^n and UV_1^n) and filtered (UV_0^{nc} and UV_1^{nc}) outputs for UV_0 and UV_1 photo-sensors. (c) shows POL-unit response for both normalized raw data and normalized filtered data. These data were acquired on 02/09/17 11:36 AM (UV-index 1, cloudy sky).

measured is about $0.6V$. When the whole sky is covered with clouds, the peak-to-peak magnitude of the UV signals drops to $0.05V$. Those weather conditions increase drastically the noise level in measured data. Heading directions ψ and $\psi + 180°$ are computed using the two local minima, here located at $78.4°$ and $258.4°$. Maxima correspond to $\psi + 90°$ and $\psi + 270°$ (fig. 3.c).

Figure 4 shows a comparison between the celestial compass and the magnetometer (LSM303D) in an outdoor area, next to our laboratory building where ferrous materials inside the walls and below the asphalt caused magnetic interferences. The robot was placed on the ground and successively turned by $10°$ until it came back to its initial position. At each step, the new heading direction is computed by the celestial compass and the magnetometer. The data were acquired under clear sky conditions, with a UV-index of 6 in April 2017. The magnetometer was calibrated so that the inner electronic parts of the robot do not disturb its measurements. The Mean Squared Error (MSE) between ground-truth and sensor measurements have been computed; the MSE of the celestial compass was of $0.25°$ while the MSE of the magnetometer reached $104.14°$ (fig. 4). These results reveal the ability of the celestial compass to provide a precise and reliable orientation when magnetometers fail.

III. THE HEXAPOD WALKING ROBOT

A. *The robot platform*

We decided to employ Hexabot (fig. 5), a fully 3D-printed, open source, six-legged walking robot based on Metabot, a four-legged walking robot [22]. Hexabot has three DYNAMIXEL XL-320 actuators per leg providing the
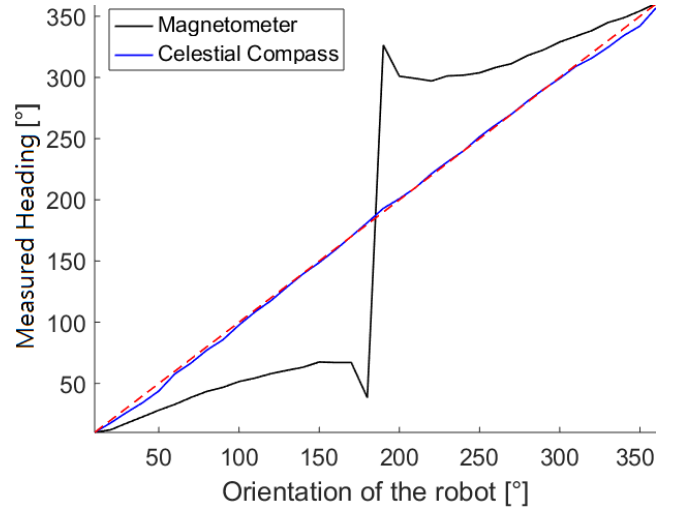

Fig. 4.   Comparison between the celestial compass and the magnetometer in an outdoor context where magnetic field interferences happen. Weather conditions : clear sky, UV-index equal to 6, April 2017.

ability to reach high walking speed (approximately $35cm/s$ in optimal conditions) and execute complex motions when crossing over an uneven terrain. Besides, six-legged robots show more stable walking movements than the four-legged ones since they can operate static gait (*i.e.* three to five legs remain in contact with the ground at any time). For instance, the tripod gait is a symmetric walking gait (three legs moving per walking step), and the wave gait consists in moving only one leg per walking step.

Previous ground-truth measurements were made in the Flying Arena of the Mediterranean (6m x 8m x 6m-height),

equipped with 17 motion-capture cameras and showed: (i) small roll and pitch average disturbances of about respectively 9.0° and 9.9° when tested at maximal speed, (ii) Hexabot is prone to heavy instantaneous disturbances in yaw orientation (up to 28.4°) [23]. During a walking task, such yaw angle errors result in an important drift from the initial trajectory.

The overall weight of Hexabot, including batteries, of 925g, and has a maximum length of 360mm and a maximum height of 145mm (fig. 5). Its battery endurance, depending on the capacity, can last up to one hour.
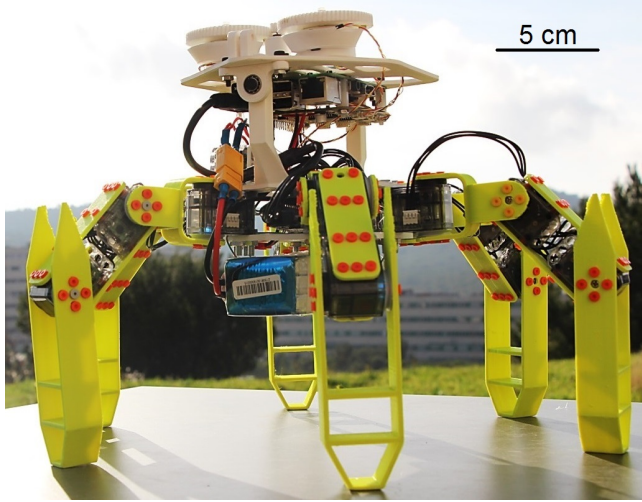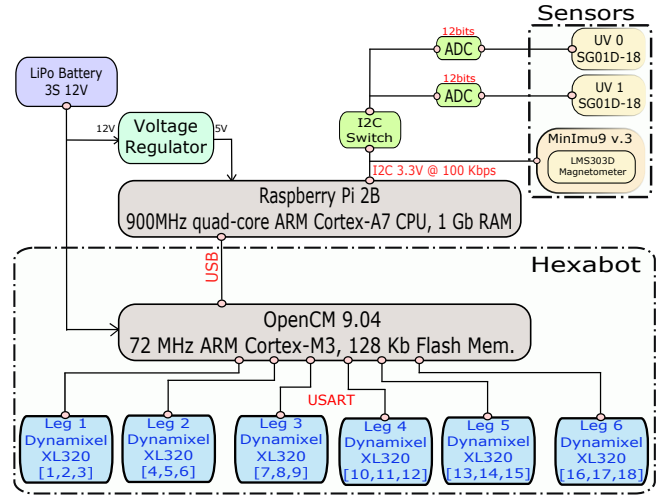

Fig. 6. Robot electronic architecture. The dashed line marks out the robot controller and actuators. The magnetometer and UV-polarized light sensors (in yellow) are connected to the Raspberry Pi 2B board using I2C communication protocol.

Fig. 5. Hexabot robot equiped with a pair of UV-polarized light sensors forming a celestial compass.

B. Robot electronic architecture

Hexabot is controlled by the OpenCM9.04C micro-controller board (based on 32-bit ARM Cortex-M3) connected to a Raspberry Pi 2B board including a 32-bit quad-core ARM Cortex-A7 processor. The Raspberry Pi board executes sensor data acquisition and processing to compute high level orders which are to be sent to the robot controller. The UV-polarized light compass is embedded on the dorsal part of the robot (fig. 2.a). Communication with the Raspberry Pi board was implemented by means of I2C protocol (fig. 6). The refresh rate of each POL-sensor is 33.3 Hz and a full acquisition time takes 42 seconds for an angular resolution set at 1.29°.

IV. EXPERIMENTS

Hexabot was set to tripod gait for all navigational tasks since it provides an optimal compromise between high walking speed and moderate attitude disturbances. However, tripod gait tend to cause an important walking direction drift over time. We propose here to use our UV-polarized light compass to contain the drift occurring after each stride. All experiments were done between 02/02/2017 and 02/20/2017 in outdoor conditions, at any time of the day, and were located in an open-air car park in the Luminy campus (43°14′01.6″N ; 5°26′39.2″E) of Aix-Marseille University, Marseille, France.

A. Heading direction recovery under various meteorological conditions

The first objective was to measure and analyze simple heading reorientation tasks under different meteorological conditions at different time of the day. The task consisted in getting the initial heading direction of the robot, then rotating it by a random yaw angle, then getting the new heading direction and compare it to the first one in order to reorientate. Once the yaw command is executed, the new heading direction was measured and compared to the initial one. All UV-polarized light measurements are compared to ground truth magnetometer measurements. To prevent any yaw angle ambiguity since the sensor response is a $\pi-$periodic sinusoidal function, yaw disturbances were set between $-70°$ and $+70°$. Such a restriction makes sense as yaw disturbances over a straight-forward walking task are systematically small and but oriented in the both direction due to interactions with the ground.

Figure 7 shows heading errors under three different weather conditions. Under clear sky conditions, the median value is of 0.4° ($n = 15$), which is twice better than the results obtained in Sahabot 1 [15] whereas the weather conditions are highly different. The peak error measured is of $-8.4°$ corresponding to a yaw disturbance of $-60°$. Under partially cloudy conditions, the median value is of $-2.9°$ ($n = 11$). The peak error measured is of $-13.8°$ ($-65°$ yaw disturbance). Finally, under cloud-covered sky conditions, the median value is of $-1.9°$ ($n = 7$) and the peak value is of $-13.9°$. To highlight these results, it should be considered that Hexabot shows an average yaw turning angle inaccuracy per stride of 8.2° with a statistical spread of 7.5° due to interactions between legs and the ground. In view of this, the presented results exhibit great performance, especially under clear sky conditions. The decrease noticed under cloudy sky and overcast sky conditions stems from the

low degree of polarization of the skylight [9] which implies the overpowering of the Rayleigh scattering, thus disturbing the polarization pattern of the skylight.
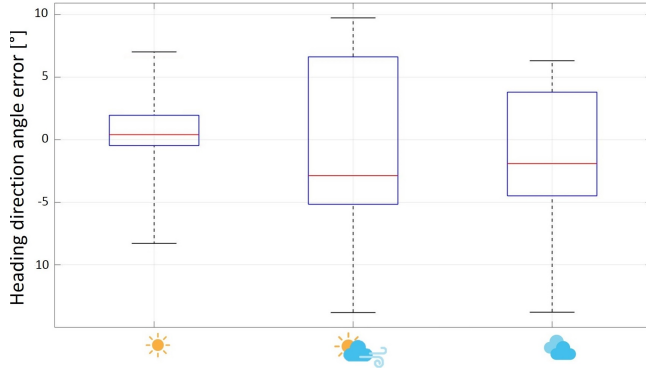

Fig. 7. Heading direction angle errors in degrees in function of weather conditions. From left to right, the median heading direction angle error measured is equal to $0.4°$ ($n = 15$), $-2.9°$ ($n = 11$), and $-1.9°$ ($n = 7$), n being the number of experiments. UV-index from 1 to 2 (Source: French Meteorological services). 42-second acquisition time per measurement.

Considering the results obtained with Sahabot robot in [15], our UV-polarized light compass provide similar and even slightly better results under clear sky, and promising results under bad meteorological conditions such as clouds in the sky and a much lower level of ultraviolet radiance due to the period and the location of experiments.

B. Heading-lock over a straight-forward walking task

Depending on various parameters such as the type of ground, the walking speed and the power supply, Hexabot shows important drifts in yaw orientation. Drift measurements were made for five straight-forward walking tasks on a flat but rough terrain. Tests were conducted over six seconds at maximum walking speed. Results show an average heading direction disturbance of $28°$ (magnetometer measurements in an outdoor terrain deprived of any magnetic field interference). In those conditions, Hexabot drifts from initial walking axis by an average length of one meter. Our UV-polarized light compass is used to limit the heading direction drift while applying yaw correction after each walking step. First, the initial direction is measured, then Hexabot executes a series of strides (a walking step) during two seconds and measures its new yaw orientation, the value of which is then compared to the initial one to compute the yaw angle correction to be applied. Hexabot executes the corresponding turning movement before moving to the next series of strides.

Due to supply limits and to prevent from the drift effect induced by the sun movements, data were acquired over two distinct days (02/18/2017 and 02/20/2017). As a result, experiments were all performed at the same time (2:00 pm) under perfectly clear sky conditions (UV index of 2). Initial heading direction was set to $220°$. Results for all experiments are shown in figure 8. An example of a walking step is shown in supplementary video.
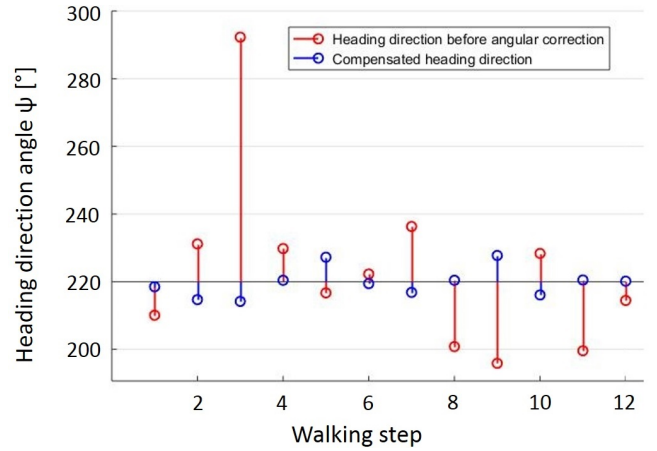

Fig. 8. Evolution of the measured heading direction angle ψ before (in red) and after (in blue) angular correction using only the UV-polarized light compass during a straight-forward walking task. Walking steps measurements from 1 to 6 were acquired on 02/18/2017 while the next six measurements were acquired on 02/20/2017.

The average heading direction angle error calculated is of $-0.3°$ which is consistent with performances exhibited previously under clear sky conditions. The peak error measured is of $7.7°$, occurring during the ninth walking step. Since there were no clouds in the sky, the polarization pattern remained rather constant all over the experiments. As a consequence, the heading direction error is mainly caused by interactions between legs and the ground.

V. CONCLUSION

In this paper, a novel insect-inspired celestial compass was presented and embedded on a walking hexapod robot to provide a new way to get the heading direction in an outdoor, open-air context, under various meteorological conditions, a low UV-index range (from 1 to 2), and at any time of the day, possibly when magnetometers fail to provide any reliable orientation measurement.

The experiments performed showed highly precise and reliable results under clear-sky conditions, with an average steady state error as small as $0.4°$. Results under cloudy-sky conditions exhibits good performances as well, from $0.8°$ under variable weather, to $1.9°$ under overcast sky, but slightly less reliable due to the high variability of meteorological conditions.

Future work will focus on the impact of the turning uncertainty of the robot on the heading direction. Residual heading-lock errors can be reduced by changing to a closed-loop system and tweaking the turning parameters of the robot. The reliability of the computation of the heading direction may also be improved by optimizing the acquisition time of the celestial compass. Finally, we will perform further studies to show the suitability of this new optical compass sensor for autonomous robotic tasks such as homing, including to find a method to fix the angular ambiguity.

REFERENCES

[1] E. Bergamini, G. Ligorio, A. Summa, G. Vannozzi, A. Cappozzo, and A. Sabatini. Estimating orientation using magnetic and inertial sensors and different sensor fusion approaches: accuracy assessment in manual and locomotion tasks, Sensors, vol. 14, no 10, pp. 18625-18649, 2014.

[2] R. Wehner, B. Michel, and P. Antonsen, Visual navigation in insects: coupling of egocentric and geocentric information, Journal of Experimental Biology, vol. 199, pp. 129-140, 1996.

[3] K.L. Coulson, Polarization and Intensity of Light in the Atmosphere, A Deepak Pub, 1988.

[4] R. Wehner, Himmelsnavigation bei Insekten, Neurophysiologie und Verhalten, Neujahrsbl Naturforsch Ges Zrich, vol. 184, pp. 1-132, 1982.

[5] T. Labhart, and E.P. Meyer, Detectors for polarized skylight in insects: a survey of ommatidial specializations in the dorsal rim area of the compound eye, Microscopy research and technique, vol. 47, no 6, pp. 368-379, 1999.

[6] T. Labhart, Polarization-opponent interneurons in the insect visual system, Nature, vol. 331, no 6155, pp. 435-437, 1988.

[7] S. Heinze, Polarized-light processing in insect brains: recent insights from the desert locust, the monarch butterfly, the cricket, and the fruit fly, In : Polarized light and polarization vision in animal sciences, Springer Berlin Heidelberg, pp. 61-111, 2014.

[8] M.V. Srinivasan, Honeybees as a model for the study of visually guided flight, navigation, and biologically inspired robotics, Physiological reviews, vol. 91, no 2, pp. 413-460, 2011.

[9] M.L. Brines, and J.L. Gould, Skylight polarization patterns and animal orientation, J. exp. Biol, vol. 96, pp. 69-91, 1982.

[10] A. Barta, and G. Horváth, Why is it advantageous for animals to detect celestial polarization in the ultraviolet? Skylight polarization under clouds and canopies is strongest in the UV, Journal of Theoretical Biology, vol. 226, no 4, pp. 429-437, 2004.

[11] T. Labhart, and E.P. Meyer, Neural mechanisms in insect navigation: polarization compass and odometer, Current opinion in neurobiology, vol. 12, no 6, pp. 707-714, 2002.

[12] S. Heinze, and U. Homberg, Linking the input to the output: new sets of neurons complement the polarization vision network in the locust central complex, Journal of Neuroscience, vol. 29, no 15, pp. 4911-4921, 2009.

[13] M. Sakura, D. Lambrinos, and T. Labhart, Polarized skylight navigation in insects: model and electrophysiology of e-vector coding by neurons in the central complex, Journal of neurophysiology, vol. 99, no 2, pp. 667-682, 2008.

[14] R. Wehner, Desert ant navigation: how miniature brains solve complex tasks, Journal of Comparative Physiology A, vol. 189, no 8, pp. 579-588, 2003.

[15] D. Lambrinos, H. Kobayashi, R. Pfeifer, M. Maris, T. Labhart and R. Wehner, An autonomous agent navigating with a polarized light compass, Adaptive Behavior, vol. 6, pp. 131-161, 1997.

[16] D. Lambrinos, R. Möller, T. Labhart, R. Pfeifer, and R. Wehner, A mobile robot employing insect strategies for navigation, Robotics and Autonomous systems, vol. 30, pp. 39-64, 2000.

[17] J. Chu, K. Zhao, Q. Zhang, and T. Wang, Construction and performance test of a novel polarization sensor for navigation, Sensors and Actuators A: Physical, vol. 148, no 1, pp. 75-82, 2008.

[18] J. Chu, H. Wang, W. Chen, and R. Li, Application of a novel polarization sensor to mobile robot navigation, Mechatronics and Automation, 2009, ICMA 2009, International Conference on. IEEE, pp. 3763-3768, 2009.

[19] J. Chu, Z. Wang, L. Guan, Z. Liu, Y. Wang, and R. Zhang, Integrated polarization dependent photodetector and its application for polarization navigation, IEEE Photonics Technol. Lett, vol. 26, no 5, p. 469-472, 2014.

[20] J. Chahl, and A. Mizutani, Biomimetic attitude and orientation sensors, IEEE Sensors Journal, vol. 12, no 2, pp. 289-297, 2012.

[21] R. Wehner, and S. Wehner, Insect navigation: use of maps or Ariadne's thread?, Ethology Ecology & Evolution, vol. 2, no 1, pp. 27-48, 1990.

[22] G. Passault, Q. Rouxel, F. Petit, and O. Ly, Metabot: a low-cost legged robotics platform for education, In : Autonomous Robot Systems and Competitions (ICARSC), 2016 International Conference on. IEEE, pp. 283-287, 2016.

[23] J. Dupeyroux, G. Passault, F. Ruffier, S. Viollet, and J. Serres, Hexabot: a small 3D-printed six-legged walking robot designed for desert ant-like navigation tasks, 20th World Congress of the International Federation of Automatic Control (IFAC), Toulouse, France, pp. 16628-16631, 2017.